

BOUSSINESQ MODELING OF WAVE TRANSFORMATION, BREAKING, AND RUNUP. II: 2D

By Qin Chen,¹ James T. Kirby,² Robert A. Dalrymple,³ Andrew B. Kennedy,⁴ and Arun Chawla⁵

ABSTRACT: In this paper, we focus on the implementation and verification of an extended Boussinesq model for surf zone hydrodynamics in two horizontal dimensions. The time-domain numerical model is based on the fully nonlinear Boussinesq equations. As described in Part I of this two-part paper, the energy dissipation due to wave breaking is modeled by introducing an eddy viscosity term into the momentum equations, with the viscosity strongly localized on the front face of the breaking waves. Wave runup on the beach is simulated using a permeable-seabed technique. We apply the model to simulate two laboratory experiments in large wave basins. They are wave transformation and breaking over a submerged circular shoal and solitary wave runup on a conical island. Satisfactory agreement is found between the numerical results and the laboratory measurements.

INTRODUCTION

An accurate model for wave-induced nearshore circulation is essential to predicting sediment and pollutant transport in coastal regions. Most of the existing numerical models for breaking-generated surf zone currents are based on vertically integrated, time-averaged (over a short-wave period) conservation laws of mass and momentum (see Svendsen and Putrevu 1995 for a review). The accuracy of such models depends on the quality of the wave transformation and breaking model that provides a circulation model with radiation stresses. Recent advances in both computer technology and dispersive, nonlinear long-wave theory (Madsen and Sørensen 1992; Nwogu 1993; Wei et al. 1995; Madsen and Schäffer 1998; Chen et al. 1998) now permit the use of Boussinesq wave models for large nearshore regions and allow the averaging of model results to predict wave-induced mean flows if wave breaking is incorporated into the model. Literature reviews on advances in Boussinesq modeling of nearshore surface gravity waves can be found in Kirby (1997) and Madsen and Schäffer (1999).

The swash zone is the interface of seawater and land. Wave runup on the beach results in swash oscillations that are believed to cause significant sediment transport (Kamphuis 1991). On the other hand, predicting wave runup on an open coast is important in estimating the area affected by storm waves and tsunamis. Liu et al. (1995), and Titov and Synolakis (1998), among others, developed numerical models for tsunami runup on the basis of nonlinear shallow water equations. Those models were tested against physical experiments carried out by Briggs et al. (1994) on solitary wave runup on a conical island. Although generally good agreement was obtained for the case of nonbreaking waves, discrepancies exist in the case of broken-wave runup, as shown by Liu et al. (1995) and Titov and Synolakis (1998). This calls for models to take nonhy-

drostatic pressure and wave breaking into account. Recently, Kobayashi (1999) provided a thorough literature review on wave runup on beaches and coastal structures and pointed out the need for research on 2D shoreline runup.

The objective of this study is to implement and validate an extended time-domain Boussinesq model for wave transformation resulting from combined refraction and diffraction, wave breaking, and wave runup in two horizontal dimensions. The model is based on the fully nonlinear Boussinesq equations introduced by Wei et al. (1995).

This paper is organized as follows. First, we describe the extension of the breaking and runup schemes constructed by Kennedy et al. (2000, hereafter referred to as Part I) to two horizontal dimensions. Next, the model is tested against Chawla and Kirby's (1996) physical experiment on wave propagation over a submerged circular shoal with and without breaking. Then, we use the measurements from Briggs et al.'s (1994) laboratory experiment of solitary wave runup on a conical island to validate the numerical model with respect to 2D shoreline runup. The results and findings are summarized in the final section.

MODEL FORMULATION

Governing Equations

The extended Boussinesq equations of Wei et al. (1995) are formulated in terms of the velocity vector $\mathbf{u}_\alpha = (u_\alpha, v_\alpha)$ at a reference elevation z_α in the water column and the free surface elevation η relative to the still water level. The equation for conservation of mass may be written as

$$\beta\eta_t + \nabla \cdot \mathbf{M} = 0 \quad (1)$$

where

$$\mathbf{M} = \Lambda \left[\mathbf{u}_\alpha + \left(\frac{z_\alpha^2}{2} - \frac{1}{6} (h^2 - h\eta + \eta^2) \right) \nabla (\nabla \cdot \mathbf{u}_\alpha) + \left(z_\alpha + \frac{1}{2} (h - \eta) \right) \nabla (\nabla \cdot (h\mathbf{u}_\alpha)) \right] \quad (2)$$

in which h is the still water depth, the subscript t denotes time differentiation, and ∇ is the horizontal gradient operator. In addition, β and Λ are introduced to account for the moving shoreline using the permeable-seabed technique. The detailed expressions of β and Λ can be found in Part I.

The equations for momentum conservation read

$$\mathbf{u}_{\alpha t} + (\mathbf{u}_\alpha \cdot \nabla) \mathbf{u}_\alpha + g \nabla \eta + \mathbf{V}_1 + \mathbf{V}_2 + \mathbf{R}_f - \mathbf{R}_b - \mathbf{R}_s = 0 \quad (3)$$

¹Postdoctoral Fellow, Ctr. for Appl. Coast. Res., Univ. of Delaware, Newark, DE 19716.

²Prof., Ctr. for Appl. Coast. Res., Univ. of Delaware, Newark, DE.

³Dir. and Prof., Ctr. for Appl. Coast. Res., Univ. of Delaware, Newark, DE.

⁴Postdoctoral Fellow, Ctr. for Appl. Coast. Res., Univ. of Delaware, Newark, DE.

⁵Grad. Student, Ctr. for Appl. Coast. Res., Univ. of Delaware, Newark, DE.

Note. Discussion open until July 1, 2000. Separate discussions should be submitted for the individual papers in this symposium. To extend the closing date one month, a written request must be filed with the ASCE Manager of Journals. The manuscript for this paper was submitted for review and possible publication on January 26, 1999. This paper is part of the *Journal of Waterway, Port, Coastal, and Ocean Engineering*, Vol. 126, No. 1, January/February, 2000. ©ASCE, ISSN 0733-950X/00/0001-0048-0056/\$8.00 + \$.50 per page. Paper No. 20145.

where g is the gravitational acceleration and \mathbf{V}_1 and \mathbf{V}_2 are the dispersive Boussinesq terms (see Wei et al. 1995 and Part I for details). In comparison with the original momentum equations of Wei et al. (1995), the additional terms \mathbf{R}_b , \mathbf{R}_{b_s} , and \mathbf{R}_s are introduced for the treatment of bottom friction, wave breaking, and subgrid lateral turbulent mixing, respectively, and will be discussed in the following subsections. It is worth mentioning that \mathbf{R}_b and \mathbf{R}_s basically act as local momentum mixing due to wave breaking and unresolved turbulence. Neither of them alters the global momentum conservation. A discussion of additional model parameters can be found in Part I.

2D Wave Breaking

Following Part I, we model the energy dissipation due to wave breaking in shallow water by introducing the momentum mixing terms \mathbf{R}_b , which are related to the second derivative of momentum flux. The associated eddy viscosity is essentially proportional to the gradient of the horizontal velocity and is strongly localized on the front face of the breaking wave. Two empirical parameters are used to determine the onset and cessation of breaking. Detailed formulation of the breaking term can be found in Part I. In comparison with the 1D breaking model, implementation of the breaking model in two horizontal dimensions requires determination of wave direction in order to estimate the age of a breaking event.

Assuming a primarily progressive wave field, the application of the Sommerfeld radiation condition ($\eta_t + \mathbf{c} \cdot \nabla \eta = 0$) on a locally constant water depth leads to an estimate of the wave celerity vector \mathbf{c} :

$$\mathbf{c} = -\frac{\eta_t}{\eta_x^2 + \eta_y^2} \nabla \eta \quad (4)$$

Accordingly, the wave incident angle θ relative to the x direction may be written as

$$\theta = \text{TAN}^{-1} \left(\frac{\eta_y}{\eta_x} \right) \quad (5)$$

Eq. 4 is in agreement with the estimate of wave celerity in Madsen et al. (1997). With knowledge of wave direction, the model can estimate the age of a breaking event at a given location by tracking the breaking history at the grid points along the wave ray. The remaining of the breaking model is essentially identical to the 1D model as detailed in Part I.

The breaking model contains four empirical coefficients. Among them are T^* , the transition time from breaking to a fully developed bore, and $\eta_t^{(i)}$ and $\eta_t^{(f)}$, which determine the onset and cessation of a breaking event. The range of typical values for the parameter $\eta_t^{(f)}$ is $0.35\sqrt{gh} \sim 0.65\sqrt{gh}$, while the other three parameters remain the same as those in Part I. The lower limit of the coefficient $\eta_t^{(i)}$ is found to be more suitable to bar/trough beaches with relatively coarser grid resolution, whereas the upper limit gives optimal agreement for waves breaking on monotonic sloping beaches. Madsen et al. (1997) reported the similar need to reduce the value of the breaking criterion for the simulation of wave breaking on the crest of a submerged bar.

Wave Runup

Instead of tracking the moving boundary during wave runup/run-down on the beach, we treat the entire computational domain as an active fluid domain by employing an improved version of the slot or permeable-seabed technique for simulation of wave runup. The original slot technique was proposed by Tao (1984). A variant of Tao's scheme has been used by Madsen et al. (1997) and Sørensen et al. (1998) in a weakly

nonlinear Boussinesq model formulated in terms of mass flux and free surface elevation.

It was shown by Madsen et al. (1997) that, even though a very narrow width of slot is used, there is still about a 10% error in the computed maximum runup in comparison with the analytical solution by Carrier and Greenspan (1958). This is attributed to the additional cross-sectional area introduced by the narrow slot because the maximum runup is very sensitive to the total volume of mass at the runup tip. In contrast to the original formulation, which did not conserve mass in the presence of a slot, we retain an equivalent cross-sectional area of a unit width of beach, leading to the improvement in the simulation of 1D runup, as shown in Part I. The extension of the runup scheme to two horizontal dimensions is straightforward. This is done by replacing the solid bottom by a narrow-slot network in the x and y directions. The resulting terms, β and Λ , in the mass equation remain identical to those in the 1D case.

Subgrid Turbulent Mixing and Bottom Friction

In large-eddy simulation of atmospheric turbulent flow, Smagorinsky-type eddy viscosity models have been widely used to account for the contribution of unresolved small-scale motions, as described in Mason (1994) and Ghosal et al. (1995). It is well known that the flow in the surf zone is characterized by eddies and turbulence generated by wave breaking. The extension of Boussinesq models based on vertically integrated Euler equations of motion to the surf zone requires inclusion of turbulence effects. In addition to the energy dissipation term due to wave breaking, which is assumed to be strongly localized on the front face of the breaking wave, a parameterization of the Reynolds-like stresses resulting from subgrid-scale turbulent processes associated with surf zone eddies may become an important factor influencing the flow pattern of the wave-generated current field. In the absence of a subgrid model in the governing equations, the underlying current field generated by wave breaking may become so chaotic that no realistic flow pattern can be recognized as observed in our numerical experiments of rip current generation on a barred beach. We therefore use a Smagorinsky-type subgrid model (Smagorinsky 1963) to account for the effect of the resultant eddy viscosity on the underlying flow. The detailed formulation is given in Chen et al. (1999).

The bottom friction is modeled by the use of the quadratic law

$$\mathbf{R}_f = \frac{f}{h + \eta} \mathbf{u}_\alpha |\mathbf{u}_\alpha| \quad (6)$$

where f is the bottom friction coefficient. In the literature, the value of f varies significantly. For instance, the coefficient used by Zelt (1991) in his Boussinesq model for solitary wave runup on a 1:20 sloping bottom is two orders of magnitude smaller than the coefficients used to compute longshore currents generated in laboratories (for example, $f \approx 1.0 \times 10^{-2}$) in Kobayashi et al. (1997). Chen et al. (1999) chose $f = 6.0 \times 10^{-3}$ in connection with the simulation of rip current generation on a barred beach with rip channels using the present model. Care should be taken when selecting bed shear stress coefficients for modeling wave-induced alongshore currents. Under field conditions, owing to the variability of hydrodynamic and morphologic characteristics, spatially variable friction coefficients (for example, $f \approx 1.0 \times 10^{-3}$ to 5.0×10^{-3}) are likely to be used, as shown by Whitford and Thornton (1996), who inferred the bed shear stress coefficients for longshore currents over a barred profile on the basis of momentum balance in alongshore direction.

Following Wei et al. (1995), quasi fourth-order finite dif-

ference schemes are used to solve the governing equations described above. An analysis of the linear stability and other properties of the numerical scheme can be found in Wei (1997).

WAVE TRANSFORMATION OVER CIRCULAR SHOAL

Model Setup

A series of physical experiments for wave transformation over a circular shoal was conducted by Chawla and Kirby (1996) in the directional wave basin at the University of Delaware. Their measurements provide good test cases for model/data comparison. Fig. 1 shows the plan view of the wave basin with the transects of wave gauge locations. The physical wave basin is approximately 18 m long and 18.2 m wide. A circular shoal was placed on an otherwise flat bottom in the basin. For detailed description of the experiment, the reader is referred to Chawla and Kirby (1996).

Accordingly, the numerical wave basin is chosen to be 20 m long and 18.2 m wide. On the western boundary, monochromatic waves are generated by the source function technique developed by Wei et al. (1999). Near the eastern wall of the wave basin, a 3 m wide sponge layer is used, which represents a sloping stone beach in the physical experiment. The center of the shoal is located at $x = 5$ m and $y = 8.98$ m. The perimeter of the shoal is given by

$$(x - 5)^2 + (y - 8.98)^2 = (2.57)^2 \quad (7)$$

and the water depth on the submerged shoal is given by

$$h = h_o + 8.73 - \sqrt{82.81 - (x - 5)^2 - (y - 8.98)^2} \quad (8)$$

in which h_o is the constant water depth of the wave basin.

Chawla and Kirby's (1996) laboratory experiments consist of test cases of regular waves and directional random waves, including breaking and nonbreaking cases. To verify the basic properties of the Boussinesq model with respect to combined refraction/diffraction and wave breaking in two horizontal dimensions, only the data sets of monochromatic waves are used in the present study. Emphasis will be given to the test case with wave breaking.

Model/Data Comparison: Nonbreaking Waves

In the case of nonbreaking wave transformation over submerged shoals, the Boussinesq model based on the fully nonlinear equations introduced by Wei et al. (1995) was verified against the laboratory experiments of Berkhoff et al. (1982) and Chawla and Kirby (1996). Excellent agreement between

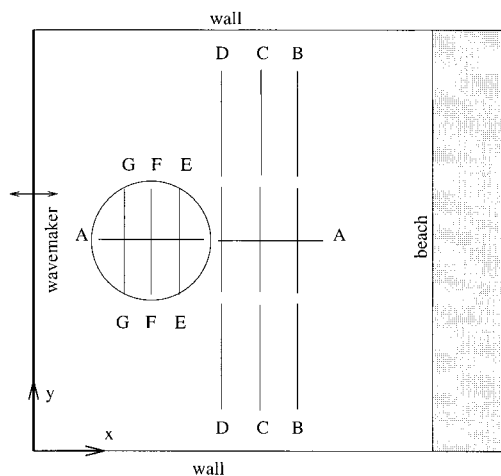


FIG. 1. Schematic View of Chawla and Kirby (1996)'s Experimental Setup and Transects of Wave Gauge Locations

the model results and measurements has been found (Wei 1997). For illustration, we present the comparison of the model results with one of Chawla and Kirby's (1996) tests (Test 4).

The wave height at the input boundary is 1.18 cm, and the wave period is 1.0 s. The flat bottom of the basin has a water depth $h_o = 45$ cm, leading to $h = 8$ cm on the top of the circular shoal. We choose the grid spacing to be 0.05 m and 0.1 m in the x (incident wave) and y directions, respectively. The time step is 0.01 s. The model is run for 40 s, and the wave field reaches a steady condition. We compute the root-mean-square (RMS) wave heights (H_{rms}) based on the time series of the last 10 s of data, although the waves are mainly periodic. Fig. 2 shows the comparison of the modeled and measured H_{rms} along seven transects covering most the areas of the submerged shoal and behind the shoal (Fig. 1). Excellent agreement is observed.

In Fig. 2, solid lines represent the Boussinesq model results while circles are the measurements, which are normalized by the incident H_{rms} . Along the longitudinal transect A-A ($y = 8.98$ m), the Boussinesq model predicts very well the wave shoaling and focusing and the decrease of wave height after the shoal. In comparison with Berkhoff et al.'s (1982) elliptical shoal, which is placed on a sloping beach, the topography in Chawla and Kirby's (1996) experiments leads to much stronger wave focusing. For instance, the maximum amplifi-

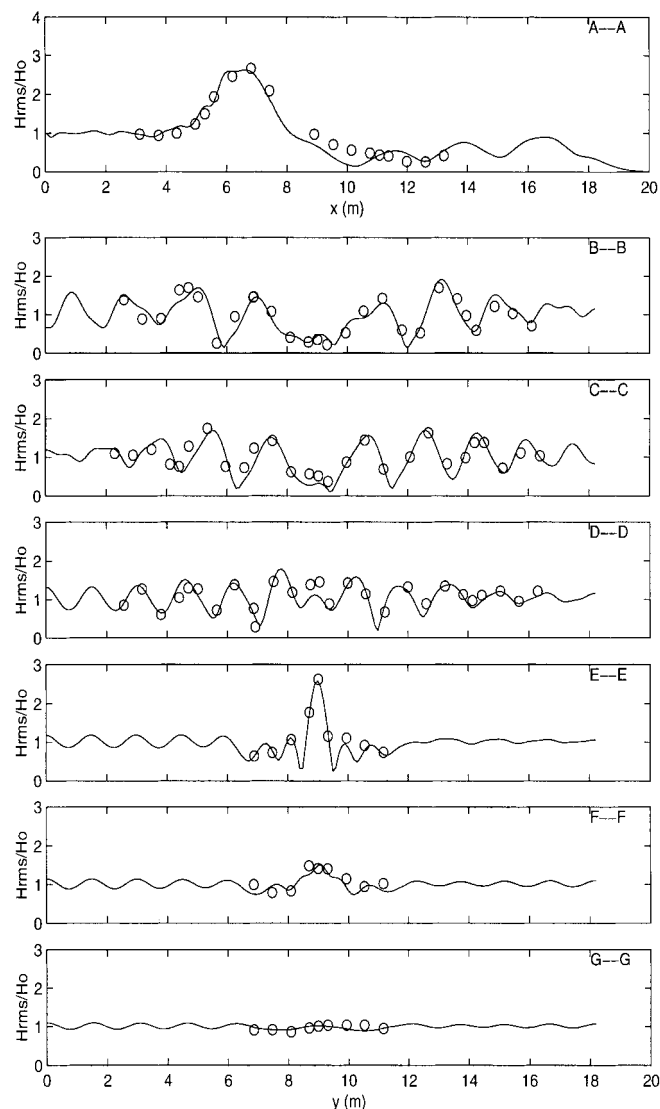


FIG. 2. Comparisons of Computed H_{rms} and Chawla and Kirby (1996)'s Measurements. Solid Lines: Model; Circles: Data. Non-breaking Waves, Test 4

cation factor of wave height reaches about 2.7 on top of the shoal in the present simulation. We notice that the Boussinesq model also correctly simulates the transverse variation of the wave field resulting from the effects of combined refraction/diffraction as shown by the good agreement along the transects from B-B to G-G. Owing to a slight off-centering of the shoal position (slightly closer to one of the side walls), the distribution of the wave height in the y direction is not symmetric. This signature of asymmetry is also accurately predicted by the Boussinesq model.

Model/Data Comparison: Breaking Waves

A more demanding test for the Boussinesq model is wave propagation and breaking over a submerged shoal. We choose another test case from Chawla and Kirby's (1996) experiment with wave breaking to verify our model. In this case, the water depth h_o is 39.5 cm. The input monochromatic wave has a 2 cm wave height and 1 s period. As the front face of a breaking/broken wave becomes very steep, finer grid size in comparison with that for the nonbreaking case is required in order to resolve the wave. Thus, we reduce the grid size in the x direction to 0.025 m, leading to about 20 grids per wave length on top of the submerged shoal, while the grid increment along the y axis and the time step remain identical to those in the case of non-breaking waves.

The Boussinesq model is run for 50 s of simulated time. To remove the effects of transients associated with the cold start of wave field and the wave breaking, we compute H_{rms} using

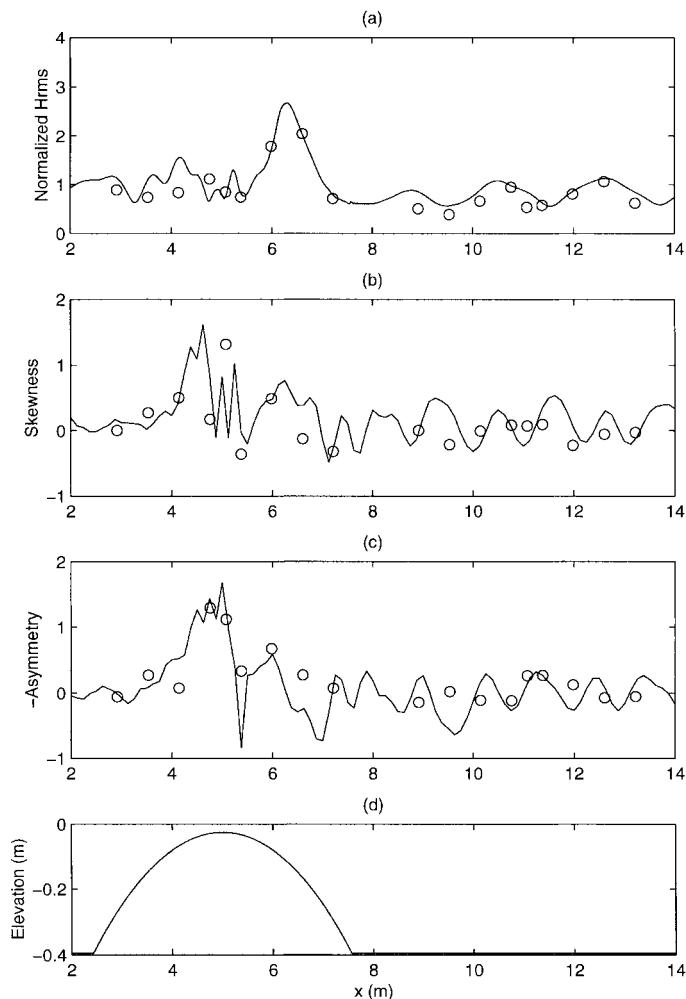


FIG. 3. Model/Data Comparisons along A-A Transect: (a) Normalized H_{rms} ; (b) Skewness; (c) Asymmetry; (d) Bottom Topography. Solid Lines: Model; Circles: Data. Breaking Waves, Test 4

the last 15 s of numerical results and the collected data. The empirical parameter $\eta_r^{(l)}$ for the wave breaking model is chosen to be the lower limit of the values indicated in the preceding section. Fig. 3 presents comparisons of the modeled results and measurements along the longitudinal transect (A-A) with respect to the normalized H_{rms} , skewness, and asymmetry (see Part I for the definition). The computed H_{rms} and third moments agree fairly well with the laboratory data.

The bottom topography along the A-A transect is shown by Fig. 3(d). Several interesting phenomena are observed from Fig. 3. First, we notice that the wave height does not reach the largest on top of the shoal but on the downward slope instead. This is attributed to the focusing effect of wave refraction on the shoal. However, the wave skewness and asymmetry appear to be the maximum near the crest of the shoal, as indicated by both the numerical and measured results. It is known that skewness and asymmetry are a measure of wave nonlinearity. Apparently, the degree of wave nonlinearity at the focusing point with the maximum wave height is weaker than that on top of the shoal, where the water depth is the minimum. Second, both depth-limited wave breaking and wave defocusing reduce the wave height. The combined decrease of wave height is much faster in comparison with the case of nonbreaking waves. Consequently, the large gradient of radiation stresses will drive horizontal circulations around the submerged shoal.

Fig. 4 depicts the data/model comparison of normalized H_{rms} along six transverse transects. On top of the shoal (F-F), agreement is fair. On the downward slope, the Boussinesq model captures the focusing effects very well, as shown by the E-E transect. Furthermore, the defocusing and diffraction

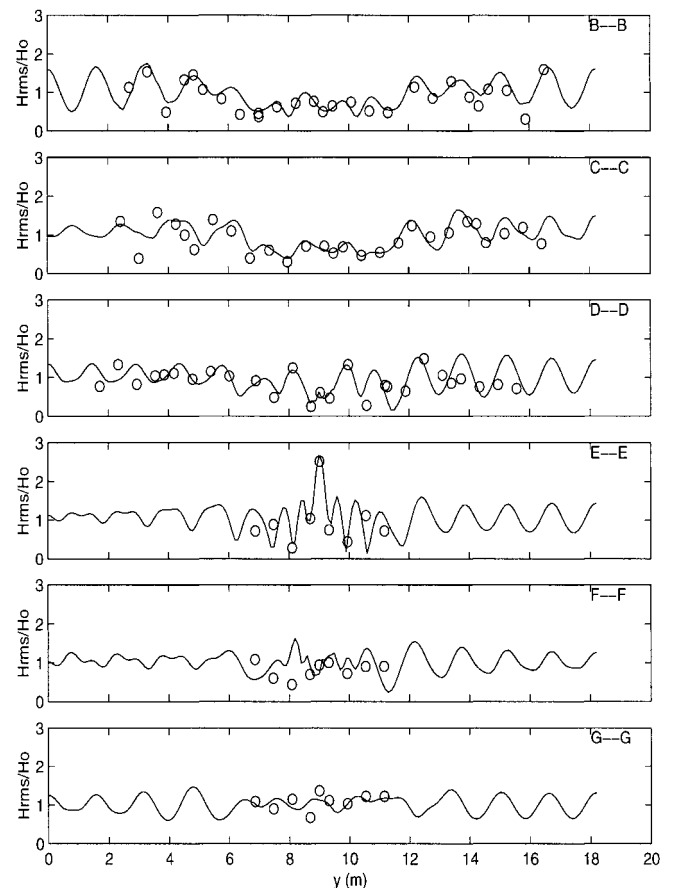


FIG. 4. Comparisons of Computed H_{rms} and Chawla and Kirby (1996)'s Measurements along Transverse Transects. Solid Lines: Model; Circles: Data. Breaking Waves, Text 4

of the broken waves behind the shoal (B-B to D-D) are also predicted reasonably well by the Boussinesq model.

A computed wave field at the end of the simulation is shown in Fig. 5(a), where the gray areas represent the modeled wave crests while the dark areas are the wave troughs. Wave crests become very peaky (narrower and brighter in the figure) on the top of the shoal due to nonlinear shoaling effects. Wave refraction over the shoal is clearly shown by the bending of wave crests on top of the shoal. Wave diffraction is also visible by the variation of wave crests in the transverse direction. It is worth mentioning that secondary wave crests are observed behind the submerged shoal due to the release of superharmonics generated by nonlinear shoaling. However, their phases may be inaccurate because of the large wave numbers of the higher harmonics at those locations. Model equations with Pade [4, 4] dispersion properties applicable to $kh = 6$ (Chen et al. 1998; Madsen and Schäffer 1998; Gobbi et al. 1999) would permit a better estimate of the released, free, higher harmonics in these two test cases.

As demonstrated by Sørensen et al. (1998) and Chen et al. (1999), Boussinesq models incorporating a treatment of wave

breaking are able to predict wave-induced horizontal currents. There is no measurement of breaking-induced circulation in Chawla and Kirby's (1996) experiments. However, a strong jet associated with wave breaking on the top of the shoal was visually observed during the experiment. Information on wave-induced circulation in the simulation can be extracted using a short averaging window to filter out the orbital wave motion. Fig. 5(b) illustrates the breaker region and the underlying current field generated by wave breaking over the shoal after 50 s have elapsed in the simulation. The current field is obtained by averaging the instantaneous fluid particle velocity at the reference level z_{α} over two wave periods. In connection with the simulation of breaking-induced currents, the bottom friction coefficient of $f = 1.0 \times 10^{-3}$ and a subgrid mixing model is used. Notice that the jetlike current tends to be unstable and vortices are likely to appear, as shown by the meandering of the computed current and the vortex pair. An account of the instability of jet-like rip currents and the mechanism of vortex generation is given in Chen et al. (1999).

The effectiveness of the breaking scheme in the case of two horizontal dimensions is demonstrated by the present test for wave breaking on a submerged circular shoal as well as the simulation of wave breaking on a barred breach with a rip channel (Chen et al. 1999). In comparison with wave breaking on a beach, simulation of wave breaking on a circular shoal is probably a more critical test for the breaking model because of the 3D nature of the breaking event. Though the occurrence of wave breaking is limited to the area on the shoal crest, the breaking event significantly affects the wave field behind the submerged shoal owing to the defocusing effect of the bathymetry, as illustrated by Fig. 5(a).

WAVE RUNUP ON CONICAL ISLAND

Briggs et al.'s (1994) laboratory experiment on solitary wave runup on a conical island has served as a benchmark for the verification of tsunami runup models (Liu et al. 1995; Titov and Synolakis 1998). We shall use the measurements from their physical experiment to validate our runup scheme for two horizontal dimensions. In the case of 1D runup, the present model was tested against an analytical solution by Carrier and Greenspan (1958) and a wide range of experimental data, including irregular waves. Good agreement has been obtained, as shown in Part I.

A schematic view of the wave basin for Briggs et al.'s (1994) experiments is shown in Fig. 6, where solitary waves are generated on the western boundary and propagate toward the eastern boundary. The wave basin is 25 m long and 30 m wide. A conical island with a slope of 1:4 is placed on an

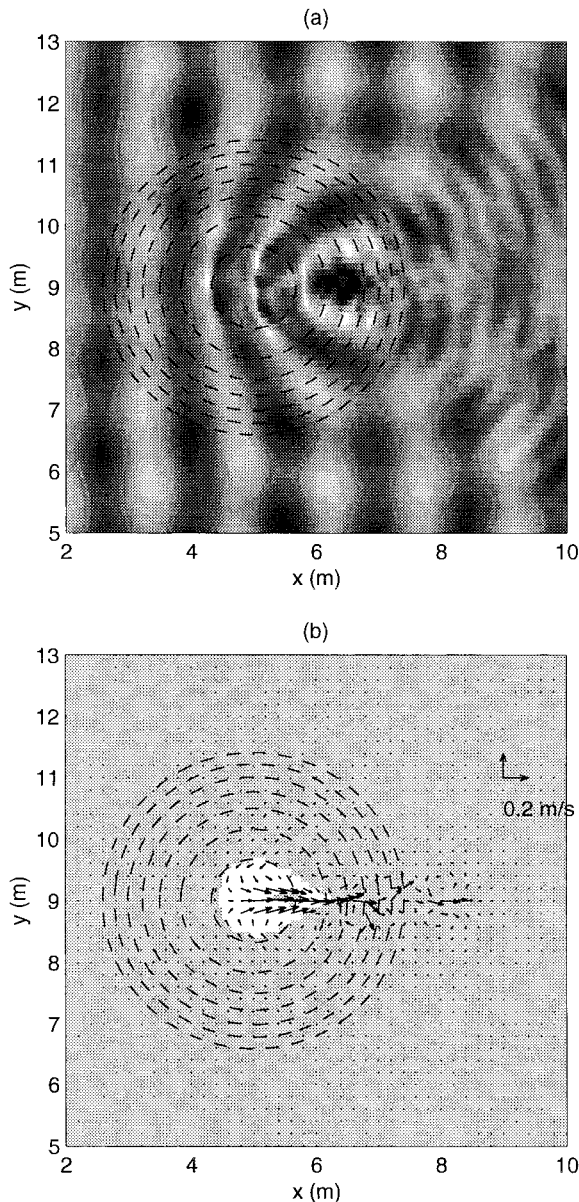


FIG. 5. Illustration of (a) Computed Wave Fields and (b) Modeled Underlying Current Field and Breaking Location (Gray Area). Dashed Lines Are Contours of Water Depth

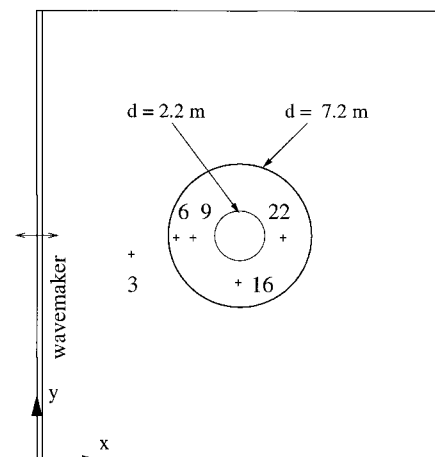


FIG. 6. Schematic of Island and Wave Gauges in Briggs et al. (1995)'s Experiment

otherwise flat bottom in the basin. The center of the island is located at $x = 13$ m and $y = 15$ m. The diameters of the island on the bottom, at the still water line, and on the top are respectively 7.2, 4.64, and 2.2 m. The water depth of the basin is 0.32 m. Further information about the experiment setup can be found in Briggs et al. (1994) and Liu et al. (1995).

There are three test cases with available data sets, including measurements of maximum runup height and free surface elevation around the island. The initial conditions for the three cases have $\epsilon = 0.05, 0.1,$ and $0.2,$ respectively, where ϵ denotes the height-to-depth ratio of the incident solitary waves. The water depth remains the same in all three cases. As pointed out by Liu et al. (1995), Case 3 is difficult to simulate because the large incident wave height leads to wave breaking on the slope of the conical island. We set up our numerical model by choosing the grid size to be 0.1 m in both x and y directions. The time step is chosen as 0.02 s. We generate solitary waves by defining the initial conditions for the model based on the analytical solutions to the Boussinesq equations with a constant water depth (Wei 1997). The crest of the solitary waves at $t = 0$ is located at $x = 0.0$. At the four lateral boundaries, closed boundaries are imposed.

Fig. 7 presents model/data comparisons of the maximum runup heights around the island for the three tests cases. The full lines represent the numerical results while stars denote the data measured by Briggs et al. (1994). The horizontal axis is the angles between the radius and the center line of the island in the incident wave direction, 0° corresponding to the front side of the island and 180° to the lee side. Runup heights are normalized by the height of the incident solitary wave. As the measurements show that the maximum runup heights are not perfectly symmetric about the center line of the island, we compare the numerical results with the average of the data on both sides of the center line aligned with the incident wave direction. Good agreement between the model predictions and the measurements is observed. The runup scheme captures the signature of 2D runup, as shown by the correct variation of

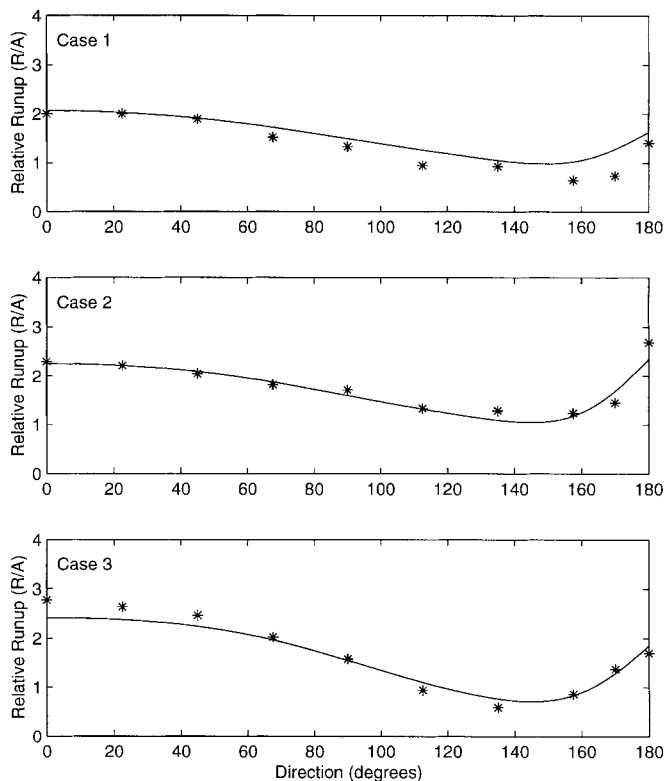


FIG. 7. Comparison of Computed and Measured Runup Heights. Stars: Measured; Solid Lines: Computed

the runup heights around the island. As mentioned above, Case 3 with broken-wave runup is a challenging test because of the inaccurate prediction by nondispersive models without the consideration of wave breaking. Although a slight discrepancy is found on front side of the island in the comparison of Case 3, the overall agreement is as good as for the nonbreaking cases.

In addition to the distribution of maximum runup heights, we compare the computed time series of free surface with the measurements at five locations. Gauge 3 is located close to the input boundary, while the other four gauges are around the island near the still water shoreline. Figs. 8, 9, and 10 show the comparisons corresponding to Cases 1, 2, and 3, respectively.

First, we notice that the computed primary waves agree reasonably well with the measurements for all three cases. The Boussinesq equations give a better description of the solitary wave than the nondispersive shallow water equations do. This becomes more clear in Case 3 when we compare our model with Titov and Synolakis' (1998) numerical results, which had remarkable discrepancies compared with the measured time series of free surface. For instance, secondary crests on the back side of the leading waves as predicted by the nondispersive model are absent in Gauges 3–16 of both the measurements and Boussinesq model results. Second, the present

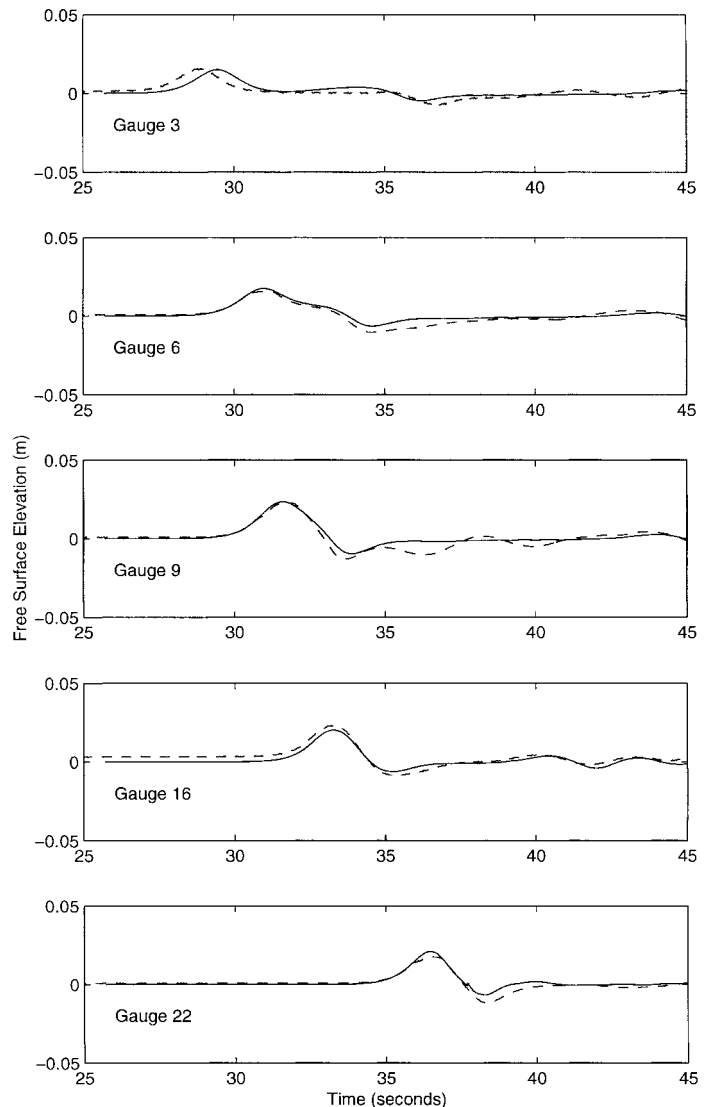


FIG. 8. Comparison of Computed and Measured Time Series of Free Surface in Case 1. Dashed Lines: Measured; Solid Lines: Computed

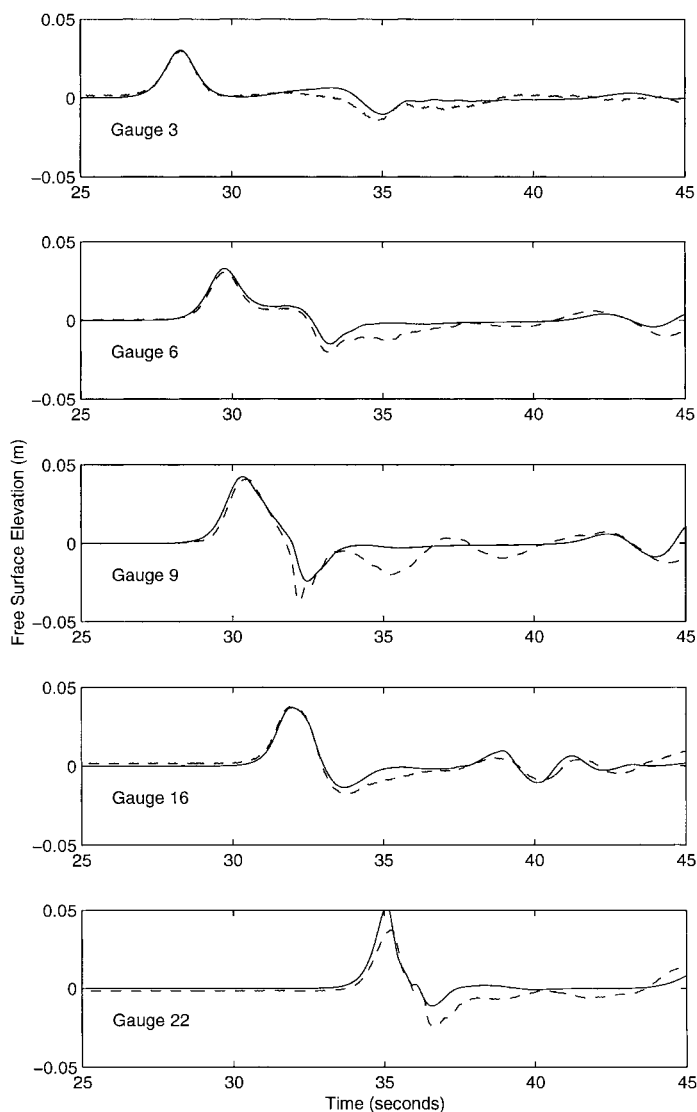


FIG. 9. Comparison of Computed and Measured Time Series of Free Surface in Case 2. Dashed Lines: Measured; Solid Lines: Computed

model predicts reasonably well the free surface on the lee side of the island, as shown by Gauge 22. In contrast, the nondispersive model tends to underestimate the leading wave height behind the island as demonstrated by Titov and Synolakis (1998). This may result from the use of overdissipative numerical schemes in the nondispersive model to implicitly account for energy dissipation by wave breaking.

The present model with permeable-seabed technique for shoreline runup, however, appears to underpredict the depression of the free surface or the reflected waves by the island. This is shown by the model/data comparison of Gauge 9, located in front of the island. The discrepancy is attributed to the slight loss of wave energy and momentum because of the presence of the narrow slot. Owing to the very steep slope of the island (1:4) and the high nonlinearity of the solitary waves in Cases 2 and 3, a slot width ten times larger than the optimal value as found in Part I is used here for the concerns of numerical instability. A low pass filter localized in the swash region is also used to suppress possible noise due to the use of a slot. It is worth mentioning that phase differences between the computed and measured free surface at Gauge 3 in Cases 1 and 3 are due to a slight variation of the gauge location in the physical experiment as pointed out in Briggs et al. (1994).

As discussed in Liu et al. (1995), a collision of the trapped

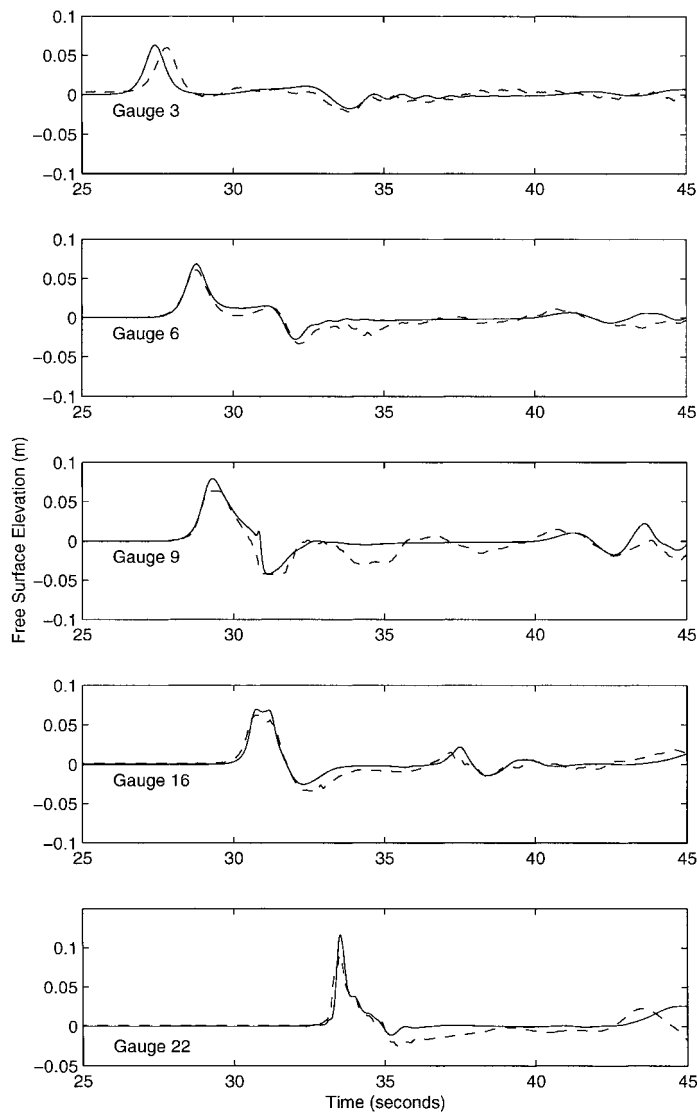


FIG. 10. Comparison of Computed and Measured Time Series of Free Surface in Case 3. Dashed Lines: Measured; Solid Lines: Computed

solitary waves on the lee side of the island could lead to a runup height, which can exceed the maximum runup on the front side of the island. Fig. 11 illustrates the collision process in Case 2. The time sequence of the computed free surface shows the scenario of head-on collision of the trapped solitary waves on the lee side of the island. Fig. 12 depicts the maximum runup on the lee side of the island in Case 3, with a larger incident solitary wave in comparison with the other two cases. It is noticed that the computed maximum water surface elevation, which is considered as the maximum runup height in Case 3, is separated from the island slope. This separation does not occur in Cases 1 and 2. As observed in the physical experiment, the collision of the trapped waves on the back side of the island in Case 3 caused wave breaking and very rough water surface. The breaking model is not expected to be able to simulate the mixing of a backward propagation bore on the lee side of the island. Nevertheless, the generally good agreement of comparisons in this section demonstrates the capability of the model for the simulation of shoreline runup in two horizontal dimensions.

SUMMARY AND CONCLUSIONS

A numerical model based on the fully nonlinear Boussinesq equations (Wei et al. 1995) has been extended to include wave

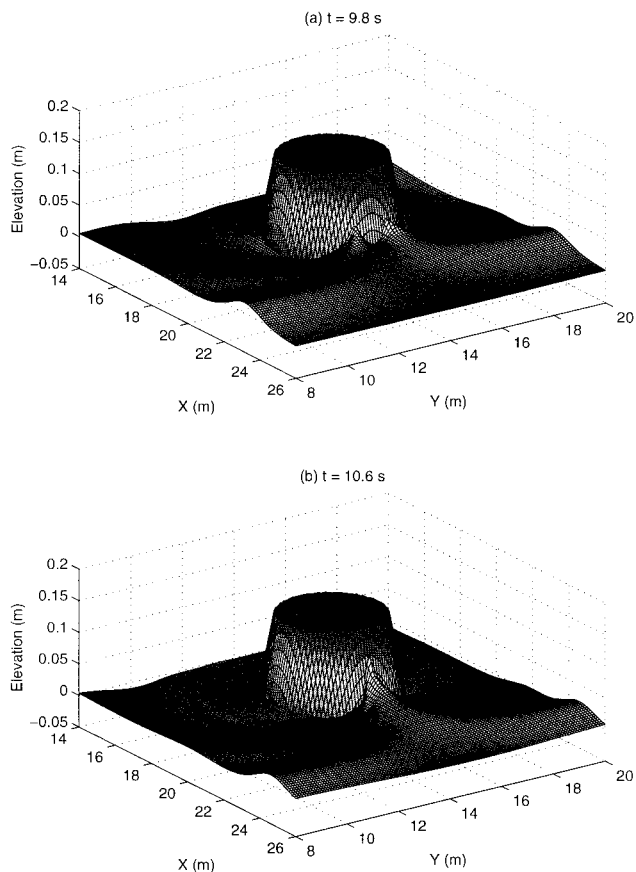


FIG. 11. Sequence of Solitary Wave Runup on Lee Side of Island in Case 2

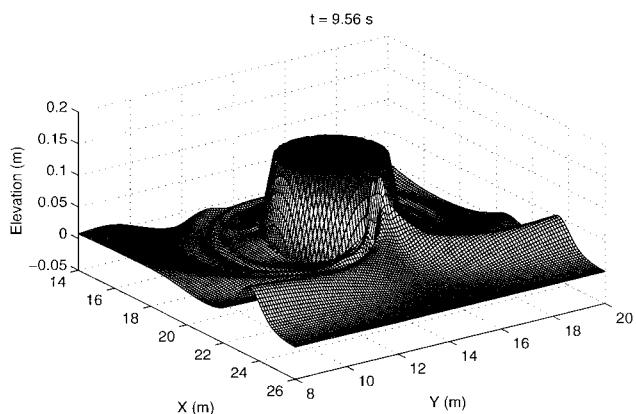


FIG. 12. Solitary Wave Runup on Lee Side of Island in Case 3

breaking and moving shorelines for the simulation of near-shore wave transformation with wave breaking, 2D swash motion and wave-induced horizontal circulation. Fully coupled wave/current interaction is taken into account by the Boussinesq equations. The model not only predicts the nearshore propagation of nonlinear surface gravity waves, but also gives the underlying unsteady flow generated by wave breaking. The current field is obtained directly by time averaging the computed instantaneous fluid particle velocity over a certain period of time.

The model results are compared with the measurements from two large-scale laboratory experiments on wave transformation over a submerged circular shoal, with and without wave breaking (Chawla and Kirby 1996), and solitary wave runup on a conical island (Briggs et al. 1994). Generally good agreement is observed between the laboratory data and the

numerical results, including spatial variation of RMS wave heights and distribution of maximum runup heights.

The numerical model predicts well the combined refraction and diffraction of nonlinear waves with wave breaking over rapidly varying bathymetry. Model/data comparisons also show that, for shoaling and runup of solitary waves, the Boussinesq model incorporating the wave breaking scheme gives better predictions than do nondispersive models based on nonlinear shallow water equations in the literature. The 2D version of the breaking and runup schemes works reasonably well. This model has been successfully used by Chen et al. (1999) to simulate a rip current system on a barred beach with rip channels in the laboratory. Good agreement has been found between numerical predictions and measurements, including wave height, mean water level, and alongshore and cross-shore currents.

ACKNOWLEDGMENTS

This study has been supported by the Office of Naval Research, Base Enhancement Program, through the research grant N00014-97-1-0283. J. T. Kirby and A. Chawla's work was also supported by the NOAA Office of Sea Grant, Department of Commerce, under Grant No. NA/6RG0162-01. Many thanks are due to Michael J. Briggs, who provided the experimental data for comparisons.

APPENDIX. REFERENCES

- Berkhoff, J. C. W., Booy, N., and Radder, A. C. (1982). "Verification of numerical wave propagation models for simple harmonic linear water waves." *Coast. Engrg.*, 6, 255–279.
- Briggs, M. J., Synolakis, C. E., and Harkins, G. S. (1994). "Tsunami runup on a conical island." *Proc., Waves—Physical and Numerical Modelling*, International Association for Hydraulic Research, Delft, The Netherlands, 446–455.
- Carrier, G. F., and Greenspan, H. P. (1958). "Water waves of finite amplitude on a sloping beach." *J. Fluid Mech.*, Cambridge, England, 4, 97–109.
- Chawla, A., and Kirby, J. T. (1996). "Wave transformation over a submerged shoal." *CACR Rep. No. 96-03*, Dept. of Civ. Engrg., University of Delaware, Newark, Del.
- Chen, Q., Dalrymple, R. A., Kirby, K. T., Kennedy, A. B., and Haller, M. C. (1999). "Boussinesq modelling of a rip current system." *J. Geophys. Res.*, 104(9), 20,617–20,637.
- Chen, Q., Madsen, P. A., Schäffer, H. A., and Basco, D. R. (1998). "Wave-current interaction based on an enhanced Boussinesq approach." *Coast. Engrg.*, 33, 11–39.
- Ghosal, S., Lund, T. S., Moin, P., and Akeselvoll, K. (1995). "A dynamic localization model for large-eddy simulation of turbulent flows." *J. Fluid Mech.*, Cambridge, England, 186, 229–255.
- Gobbi, M. F., Kirby, J. T., and Wei, G. (1999). "A fully nonlinear Boussinesq model for surface waves. II: Extension to $O(kh^4)$." *J. Fluid Mech.*, Cambridge, England, in press.
- Kamphuis, J. W. (1991). "Alongshore sediment transport rate." *J. Wtrwy., Port, Coast., and Oc. Engrg.*, ASCE, 117(6), 624–640.
- Kennedy, A. B., Chen, Q., Kirby, J. T., and Dalrymple, R. A. (2000). "Boussinesq modelling of wave transformation, breaking, and runup. I: 1D." *J. Wtrwy., Port, Coast., and Oc. Engrg.*, ASCE, 126(1), 39–47.
- Kirby, J. T. (1997). "Nonlinear, dispersive long waves in water of variable depth." *Gravity waves in water of finite depth*, J. N. Hunt, ed., Computational Mechanics Publications, Boston, 55–126.
- Kobayashi, N. (1999). "Wave runup and overtopping on beaches and coastal structures." *Advances in coastal and ocean engineering*, P. L.-F. Liu, ed., World Scientific, River Edge, N.J.
- Kobayashi, N., Karjadi, E. A., and Johnson, B. D. (1997). "Dispersion effects on longshore currents in surf zones." *J. Wtrwy., Port, Coast., and Oc. Engrg.*, ASCE, 123(5), 240–248.
- Liu, P. L.-F., Cho, Y.-S., Briggs, M. J., Kanoglu, U., and Synolakis, C. E. (1995). "Runup of solitary waves on a circular island." *J. Fluid Mech.*, Cambridge, England, 302, 259–285.
- Madsen, P. A., and Schäffer, H. A. (1999). "A review of Boussinesq-type equations for gravity waves." *Advances in coastal and ocean engineering*, P. L.-F. Liu, ed., World Scientific, River Edge, N.J.
- Madsen, P. A., and Schäffer, H. A. (1998). "Higher order Boussinesq-type equations for surface gravity waves: Derivation and analysis." *Philosophical Trans. Royal Soc., London, Ser. A.*, 356, 1–59.

- Madsen, P. A., and Sørensen, O. R. (1992). "A new form of the Boussinesq equations with improved linear dispersion characteristics. Part 2: A slowly varying bathymetry." *Coast. Engrg.*, 18, 183–204.
- Madsen, P. A., Sørensen, O. R., and Schäffer, H. A. (1997). "Surf zone dynamics simulated by a Boussinesq-type model. Part I: Model description and cross-shore motion of regular waves." *Coast. Engrg.*, 32, 255–287.
- Mason, P. (1994). "Large-eddy simulation: A critical review of the technique." *Quarterly J. Royal Meteorological Society*, Bracknell, England, 120, 1–26.
- Nwogu, O. (1993). "Alternative form of Boussinesq equations for near-shore wave propagation." *J. Wtrwy., Port, Coast., and Oc. Engrg.*, ASCE, 119(6), 618–638.
- Smagorinsky, J. (1963). "General circulation experiments with the primitive equations. I. The basic experiment." *Monthly Weather Rev.*, 91, 99–165.
- Sørensen, O. R., Schäffer, H. A., and Madsen, P. A. (1998). "Surf zone dynamics simulated by a Boussinesq-type model. III: Wave-induced horizontal nearshore circulations." *Coast. Engrg.*, 33, 155–176.
- Svendsen, I. A., and Putrevu, U. (1995). "Surf-zone hydrodynamics." in *Advances in coastal and ocean engineering*, P. L.-F. Liu, ed., 2, 1–78.
- Tao, J. (1984). "Numerical modelling of wave runup and breaking on the beach." *Acta Oceanologica Sinica*, Beijing, 6(5), 692–700 (in Chinese).
- Titov, V. V., and Synolakis, C. E. (1998). "Numerical modeling of tidal wave runup." *J. Wtrwy., Port, Coast., and Oc. Engrg.*, ASCE, 124(4), 157–171.
- Wei, G. (1997). "Simulation of water waves by Boussinesq models," PhD thesis, Dept. of Civ. Engrg., University of Delaware, Newark, Del.
- Wei, G., Kirby, J. T., Grilli, S. T., and Subramanya, R. (1995). "A fully nonlinear Boussinesq model for surface waves. Part I: Highly nonlinear unsteady waves." *J. Fluid Mech.*, Cambridge, England, 294, 71–92.
- Wei, G., Kirby, J. T., and Sinha, A. (1999). "Generation of waves in Boussinesq models using a source function method." *Coast. Engrg.*, 36, 271–299.
- Whitford, D. J., and Thornton, E. B. (1996). "Bed shear stress coefficients for longshore currents over a barred profile." *Coast. Engrg.*, 27, 243–262.
- Zelt, J. A. (1991). "The run-up of nonbreaking and breaking solitary waves." *Coast. Engrg.*, 15, 205–246.